(Received 10 December 2023, Accepted 18 January 2024, Scheduled 30 January 2024)

A Low-Profile UHF RFID Tag Antenna Loaded with Rectangular Loop for Double-Sided Anti-Metal Applications

Jinhao Wang and Jiade Yuan*

College of Physics and Information Engineering, Fuzhou University, Fuzhou 350300, China

ABSTRACT: A low-profile ultra-high frequency (UHF) radio frequency identification (RFID) tag antenna for double-sided anti-metal applications is proposed. The antenna comprises a middle layer of radiation patch, which is sandwiched between two layers of foam substrates, each with a thickness of 0.5 mm, and flanked by two layers of ground plane. A rectangular loop is designed on the radiation patch to expand the frequency band and optimize impedance matching. Particularly, one side of the radiation patch is shorted to the ground through a slotted stub to reduce the antenna size. The tag antenna is compact with a dimension of 38 mm $\times$ 20 mm $\times$ 1.15 mm ($0.1159\lambda \times 0.061\lambda \times 0.0035\lambda$ at 915 MHz). When the two ground planes are individually mounted on metallic objects, the read distances are 5.4 m and 5.2 m, respectively. The proposed tag antenna demonstrates double-sided metal resistance, making it highly suitable for use in the industrial internet of things field.

1. INTRODUCTION

Radio frequency identification (RFID) is a contactless, short-range automatic identification technology. Its core principle is the use of radio frequency signals for tag identification and data exchange [1]. RFID technology offers advantages such as strong interference resistance, high storage capacity, contactless operation, long lifespan, capability for multi-tag recognition, and fast response [2]. In practical applications, the UHF RFID tag antennas need to be placed on objects of various materials and sizes. Traditional dipole antennas typically do not function properly when being placed on metal objects [3].

To mitigate the effects of the metal environment on the performance of tag antennas, extensive researches have been conducted on anti-metal tag antennas. For instance, employing artificial magnetic conductors (AMCs) instead of metal ground planes or incorporating electromagnetic bandgap (EBG) structures can effectively suppress surface waves, reduce metal electromagnetic interference, and minimize the effects of metal backing on tag antenna performance [4, 5]. However, this method significantly increases the size, complexity, and cost of the tag antenna. In addition, there are planar inverted-F antennas (PIFAs) and microstrip patch antennas, which use a metal ground plane to isolate the tag antenna from the metal environment [6, 7]. In [8], dual planar inverted-F antennas are arranged in a cross pattern to achieve directional insensitivity. However, the tag size is relatively large, and the tuning process is cumbersome, attributed to sensitivity to the location of vias. To alleviate the above issues, folded patch antennas have been proposed to simplify the antenna tuning process and reduce size. In [9, 10], multiple slots or meandering slotlines are employed to reduce the size of the tag antenna. In [11], a serrated patch radiator is used to fine-tune the resonant frequency of the tag antenna. In [12], a T-shaped matching network is utilized for impedance matching, enhancing the antenna's gain. In [13], the coupling between complementary placed coupled C-shaped patches generates sufficient reactance for impedance matching. In [14], short stubs are used to extend the antenna's bandwidth. These techniques eliminate the need for additional printed circuit board to create shorted vias, making the tuning simpler and the fabrication more straightforward.

The above tag antennas are all used for anti-metal, but they must touch the metal object with a specific side during use. In some application scenarios where tags need to be hung on metal objects, it may be inconvenient for users to distinguish which side touch the metal object, or incorrect hanging may result in tag disability. In such scenarios, the tag antenna for anti-metal used on both sides can overcome the inconvenience in use. In [15], a double-sided anti-metal tag antenna using a loop structure for impedance matching is proposed. In [16], a double-sided anti-metal tag consisting of three nested deformable rings is proposed. However, the thickness of the double-sided anti-metal tags is relatively large.

In this paper, a low-profile double-sided anti-metal tag antenna is proposed. The proposed tag antenna features two symmetrical metal grounds, enabling either side to be placed on metal objects. By loading a rectangular loop and shorting stubs, the antenna exhibits a compact size with a footprint of approximately 0.1λ. Most importantly, even with its diminutive dimensions, the antenna can provide sufficient resistance and inductance for conjugate matching with the chip, achieving excellent power transfer coefficient (PTC) and an extended reading distance.

* Corresponding author: Jiade Yuan (yuanjiade@fzu.edu.cn).

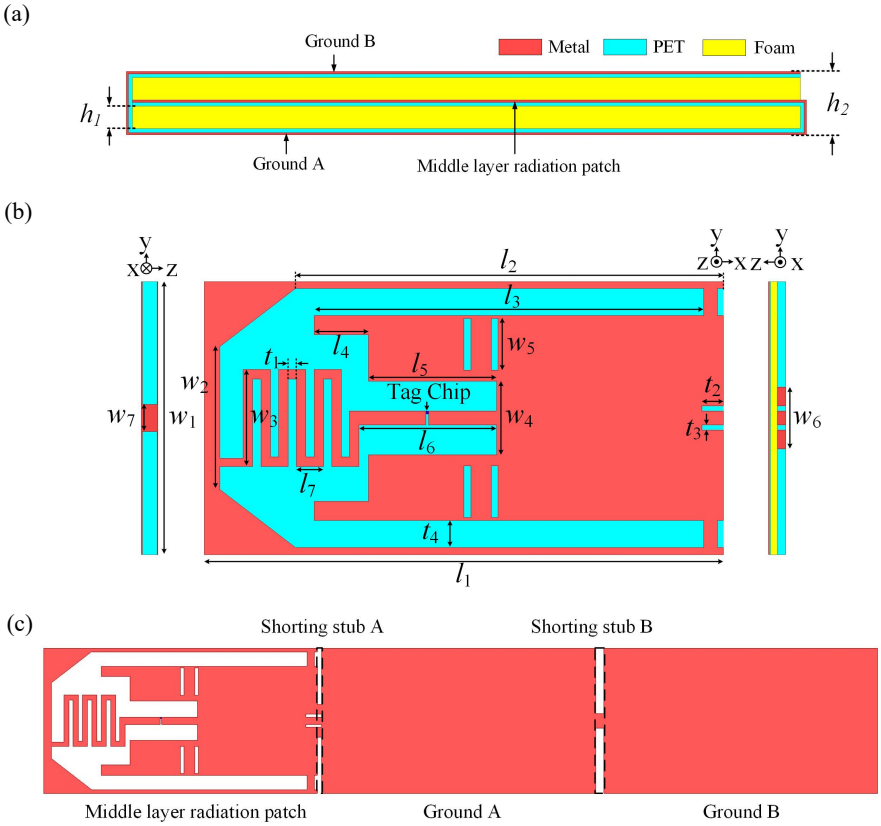

FIGURE 1. Configuration of the proposed tag antenna. (a) Cross-sectional view. (b) Middle layer radiation patch and side views. (c) Naked inlay. The parameters are $l_1 = 38$, $l_2 = 31.4$, $l_3 = 28.6$, $l_4 = 4$, $l_5 = 9.4$, $l_6 = 10.1$, $l_7 = 2$, $w_1 = 20$, $w_2 = 10.5$, $w_3 = 7.1$, $w_4 = 5.4$, $w_5 = 3.8$, $w_6 = 4.5$, $w_7 = 2$, $t_1 = 0.6$, $t_2 = 1.6$, $t_3 = 0.4$, $t_4 = 2$, $h_1 = 0.5$, $h_2 = 1.15$ (unit: mm).

2. ANTENNA STRUCTURE AND ANALYSIS

2.1. Antenna Structure

Figure 1 shows the configuration of the proposed tag antenna. The antenna is fabricated by etching the aluminum foil on the substrate of a flexible polyethylene terephthalate (PET) with a thickness of 0.05 mm. Fig. 1(a) depicts the cross-sectional view, it consists of three metallic layers separated by two layers of foam substrates. The middle layer is the radiation patch, named as the middle layer radiation patch. The top and bottom layers are two metal grounds, named as Ground A and Ground B, respectively. The middle layer radiation patch consists of a U-shaped patch, bent arm, and a rectangular loop, as depicted in Fig. 1(b). The tag chip, a MW8112 from MAXWAVE MICRO Co., Ltd., is positioned at the junction of the bent arm and the U-shaped patch. The chip has a reading sensitivity of -20 dBm and an impedance of $18 - j253\,\Omega$ at 915 MHz. Ground A and Ground B are rectangular patches with identical structural dimensions. The middle layer radiation patch is connected to the Ground A through the shorting stub A on the right side, where two slots are etched on the shorting stub A and extend towards the middle layer radiation patch. Ground A and Ground B are connected through the shorting stub B on the left side. A naked inlay before folding is shown in Fig. 1(c).

The middle layer radiation patch, Ground A, and Ground B are folded and wrapped around two pieces of 0.5 mm-thick polyethylene foam ($\varepsilon_r = 1.12$, $\tan\delta = 0.0001$). The flexible foam not only serves as structural support to maintain the shape of the tag but also isolates the three layers of metal. The folding procedure is as follows: First, a foam is placed upon Ground A, and then the middle layer radiation patch is folded to cover it. Finally, another foam is placed on top of the middle layer radiation patch, and Ground B is folded to cover the foam.

The proposed tag antenna has two possible operating states. When Ground A touches the metal plate, the middle layer radiation patch and Ground B act as the radiators, named as the TA state. Similarly, when Ground B touches the metal plate, the middle layer radiation patch and Ground A act as the radiators, named as the TB state.

2.2. Design Analysis

Analysis starts with the rectangular loop in the middle layer radiation patch. Fig. 2(a) shows the effects of with and without rectangular loop on reflection amplitude S_{11}. The performance of the RFID tag antenna within the bandwidth where $S_{11} < -3$ dB is considered acceptable [17]. Therefore, the -3 dB bandwidth can be used as a criterion for evaluating its bandwidth. In the left inset of Fig. 2(a), the antenna is without a rectangular loop, and the S_{11} bandwidth appears relatively narrow, with minimum S_{11} values reaching only -6 dB. After loading the rectangular loop, as shown in the right inset of Fig. 2(a), the bandwidth significantly widens, increasing

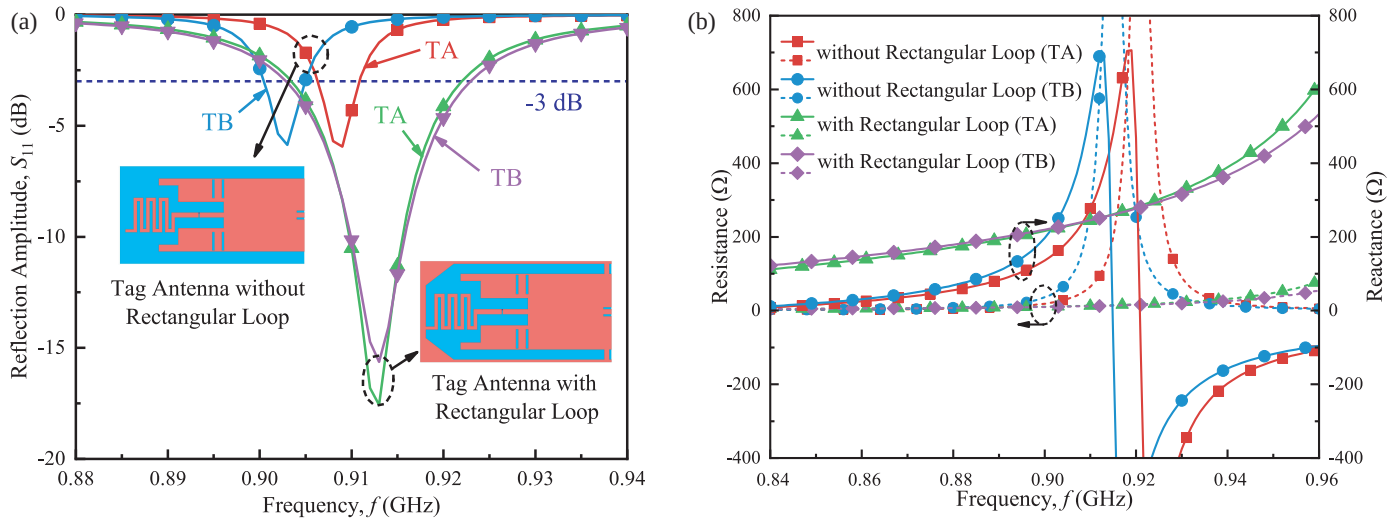

FIGURE 2. The effects on tag antenna performance with and without the rectangular loop. (a) Reflection amplitude S_{11}. (b) Resistance and reactance.

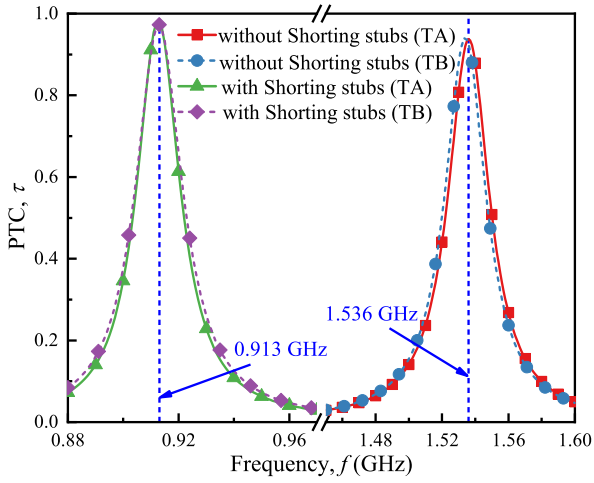

FIGURE 3. The effects of with and without the shorting stubs on the PTC of the tag antenna.

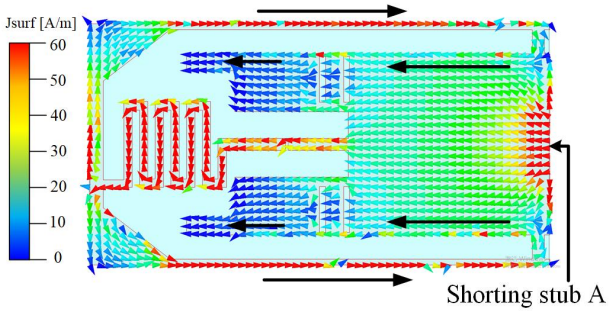

FIGURE 4. Surface currents distribution of the proposed tag antenna at 913 MHz.

by about 5 times compared to when the rectangular loop is not loaded. Meanwhile, the minimum values of S_{11} for both the TA and TB states are less than -15 dB. This indicates that the proposed rectangular loop has significant advantages in extending the antenna bandwidth and optimizing impedance matching.

Figure 2(b) shows the resistance and reactance of the tag antenna with and without the rectangular loop. Compared to the configuration without the rectangular loop, the introduction of the rectangular loop results in a smoother variation of resistance and reactance with frequency. When the antenna impedance exhibits slow and stable variation, it enables the antenna and the chip to maintain a good impedance match over a wider frequency range. At this stage, the proposed tag antenna in TA and TB states exhibits almost identical operational performance.

Analysis continues with two shorting stubs, namely Shorting stub A and Shorting stub B. The PTC is used to measure the impedance matching between the tag antenna and the tag microchip, it can be calculated as $\tau = 4R_cR_a/|Z_c + Z_a|^2$ [18]. Fig. 3 shows the effects of with and without the shorting stubs on the PTC of the tag antenna. When the antenna is without loading the two shorting stubs, the resonant frequency corresponding to the maximum PTC value is 1.536 GHz. After loading two shorting stubs, the resonant frequency drops to 0.913 GHz. The reason can be explained as these two shorting stubs guide surface currents from the radiation patch to the ground, lengthening the current path and thereby decreasing the antenna's resonant frequency. Therefore, to keep the resonant frequency unchanged, incorporating two shorting stubs can effectively reduce the required size of the antenna. Additionally, two slots are etched on the shorting stub A to fine tune the resonance frequency.

Figure 4 depicts the simulated surface current distribution on the tag antenna at 913 MHz. It is observed that there is strong current flowing along shorting stub A, indicating that shorting stub A is highly reactive and can be effective in tuning the resonant frequency of the antenna. The currents along the edges

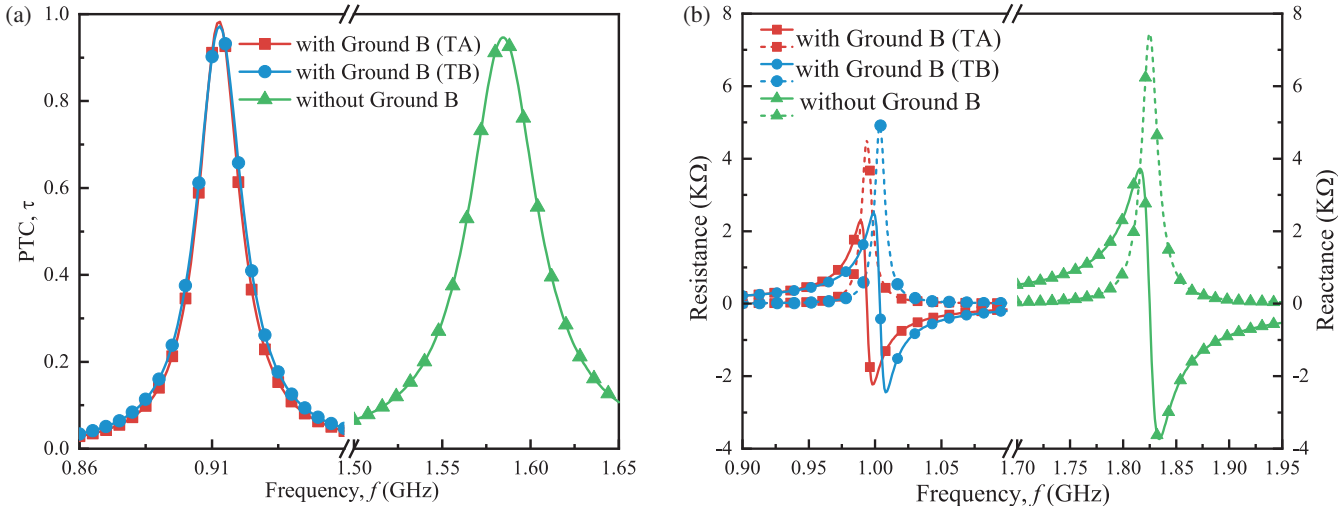

FIGURE 5. The effects on tag antenna performance with and without the Ground B. (a) PTC. (b) Resistance and reactance.

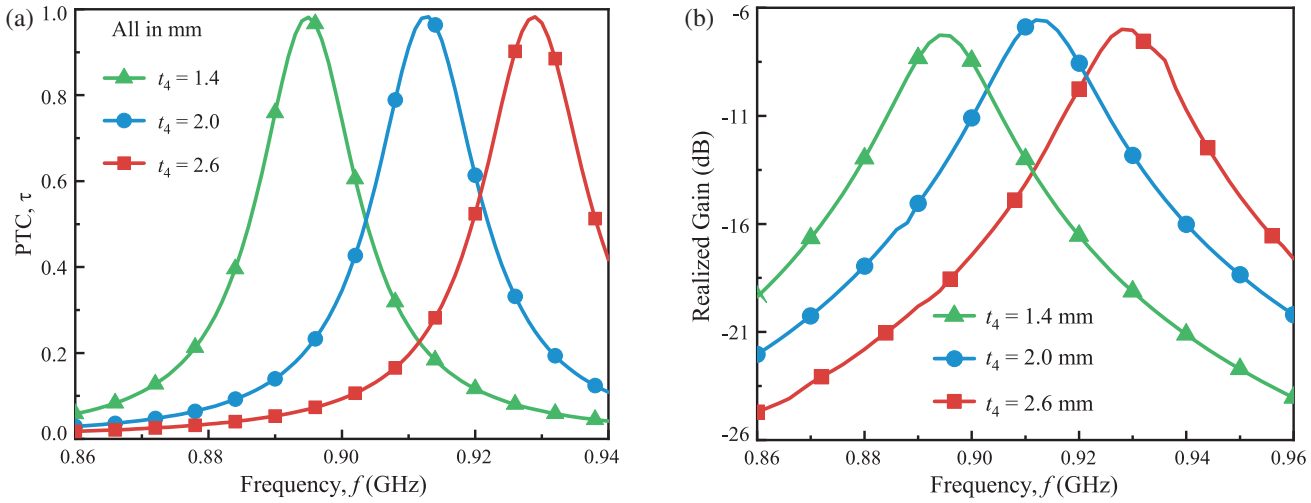

FIGURE 6. The effects of t_4 on the (a) PTC (TA) and (b) realized gain (TA).

of the gap between the outer rectangular loop and the central U-shaped patch are opposite, representing a salient feature of mutual coupling between the patches.

Figure 5 shows the effects of with and without Ground B on the tag antenna's PTC and impedance. When the tag antenna is without Ground B, the antenna's resonant frequency is 1.584 GHz. With the addition of Ground B, the resonant frequency decreases by 671 MHz, and the PTC slightly increases. Therefore, Ground B can effectively lower the antenna's resonant frequency without affecting the impedance matching of the tag antenna, thus achieving the characteristics of double-sided anti-metal.

2.3. Parametric Studies

Parametric studies are performed through HFSS simulations to examine the effects of the antenna parameters on PTC, realized gain, and impedance for the antenna design and optimization. To validate the anti-metal property, the tag antenna is simulated over a 200 mm × 200 mm metal plate. The TA and TB states exhibit consistent changing trends, so only the TA state is discussed.

The effects of the gap (t_4) between the rectangular loop and the U-shaped patch on the PTC and realized gain are shown in Fig. 6. It can be observed that as t_4 decreases from 2.6 mm to 1.4 mm, the resonant frequency gradually shifts towards lower frequencies. From Fig. 6(b), it is seen that the tag antenna has the maximum realized gain when $t_4 = 2.0$ mm. This is because when $t_4 = 2.0$ mm, the rectangular loop and the U-shaped patch mutually couple, creating sufficient reactance, which lowers the resonant frequency and increases the realized gain. Therefore, by adjusting the gap t_4, the resonant frequency of the tag antenna can be tuned without compromising the PTC.

The next study explores the effects of the bent arm width (w_3), as shown in Figs. 7(a) and (b). When w_3 increases from

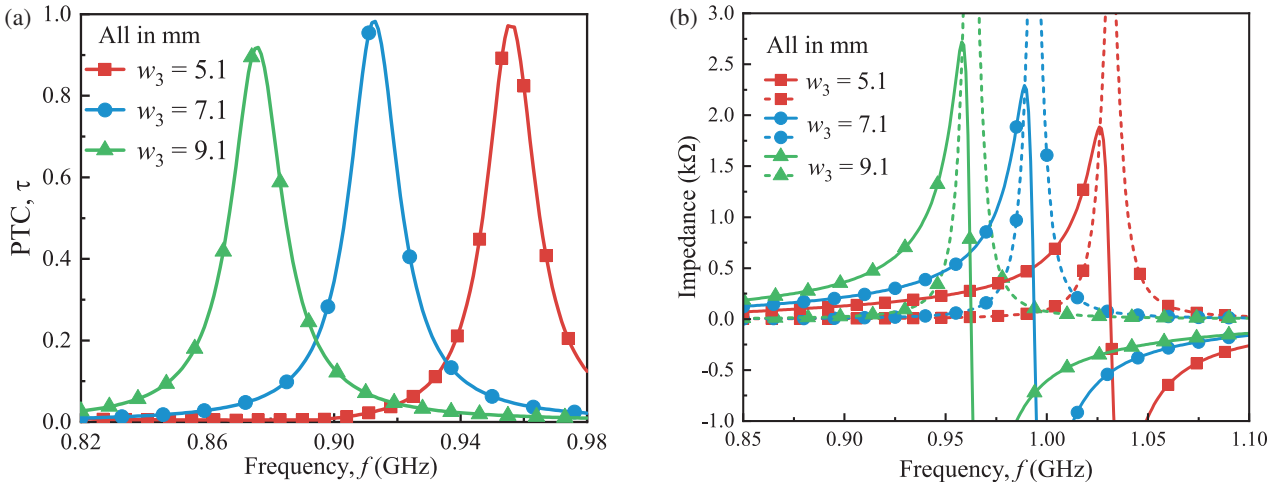

FIGURE 7. The effects of w_3 on the (a) PTC (TA) and (b) impedance (TA).

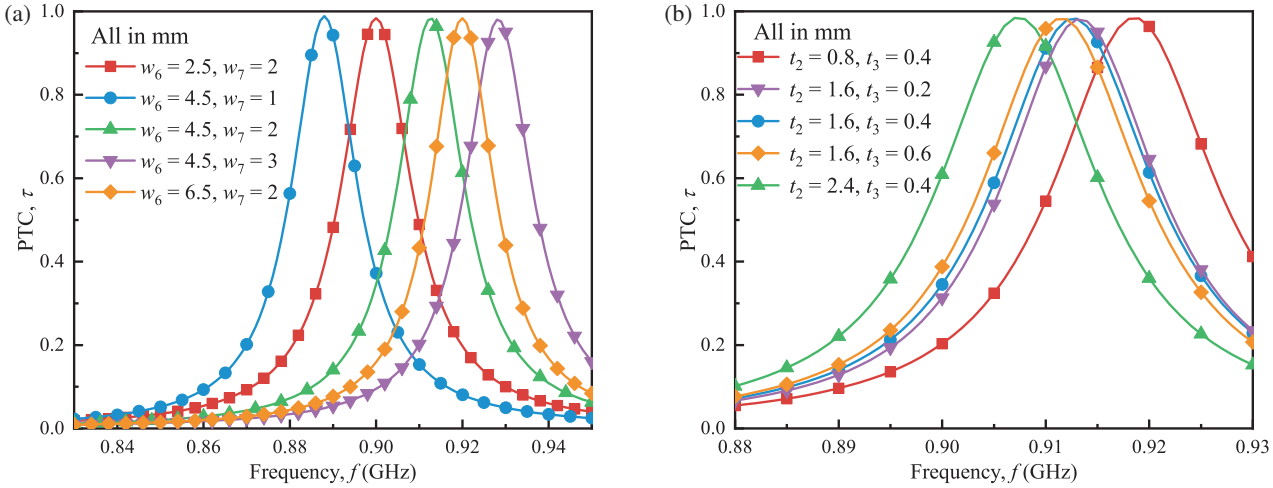

FIGURE 8. (a) The effects of w_6 and w_7 on the PTC (TA). (b) The effects of t_2 and t_3 on the PTC (TA).

5.1 mm to 9.1 mm, the resonant frequency of the tag antenna gradually decreases within the range of 820–980 MHz, while the resistance and reactance exhibit increasing trend. This can be explained that increasing w_3 can extend the current path, thereby lowering the resonant frequency. The tag antenna with $w_3 = 7.1$ mm can achieve a good PTC at 913 MHz.

Figure 8 shows the effects of w_6, w_7, t_2, and t_3 on the PTC. As w_6 and w_7 increase, the resonant frequency of the tag antenna shifts towards higher frequencies. Conversely, when t_2 and t_3 increase, the resonant frequency shifts towards lower frequencies. These parameter variations have almost no effect on PTC. Therefore, w_6 and w_7 allow for significant adjustment of the resonant frequency, while t_2 and t_3 enable fine-tuning of the resonant frequency.

3. RESULTS AND DISCUSSION

The fabricated naked inlay and final prototype are shown in Fig. 9(a). Fig. 9(b) shows the test scenario of the Voyantic Tagformance measurement system [19]. The effective-isotropic-radiation-power (EIRP) is fixed 3.28 W for the subsequent measurments. During the test, the tag antenna is placed between RFID reader and a 200 mm × 200 mm metal plate for evaluation.

The realized gains of the tag antenna in simulation and measurement are shown in Fig. 10. It can be observed that the measured realized gains within the frequency range of 860–960 MHz almost matche the simulated realized gains trend. The simulated maximum realized gains are −7.6 dB (TA) and −7.7 dB (TB) at 913 MHz, while the measured maximum realized gains are −8.8 dB (TA) and −9.1 dB (TB) at 910 MHz. The measured results are slightly smaller than the simulated results. This deviation is caused by antenna simulation, manufacturing, and measurement errors.

The read distance (R) of the tag antenna can be calculated using the Friis transmission equation [24]. P_{EIRP} represents the equivalent isotropic radiated power of the reader, which is

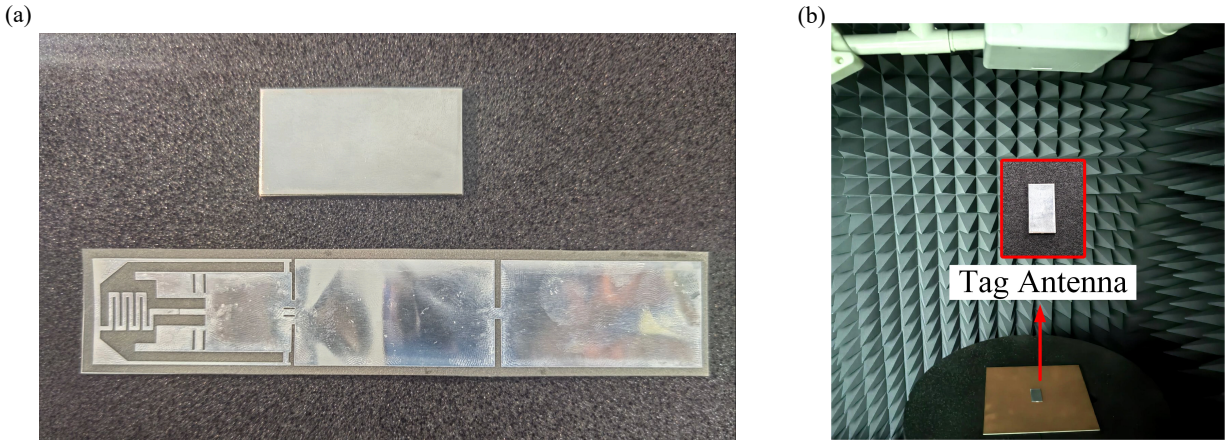

FIGURE 9. (a) Folded and pre-folded of the proposed tag antenna. (b) Test scenario of the Voyantic Tagformance.

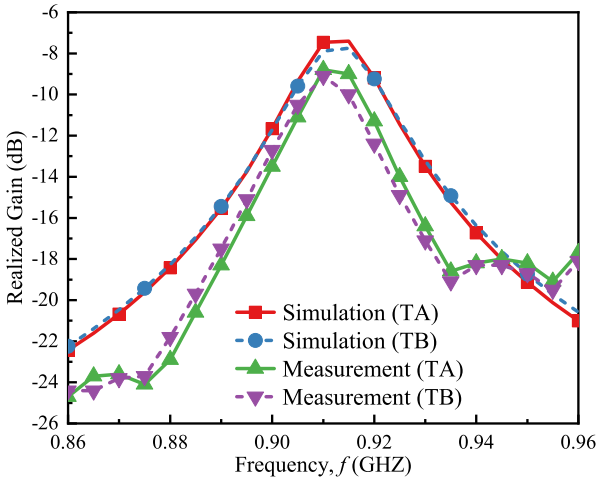

FIGURE 10. Measured and simulated realized gains of the proposed tag antenna.

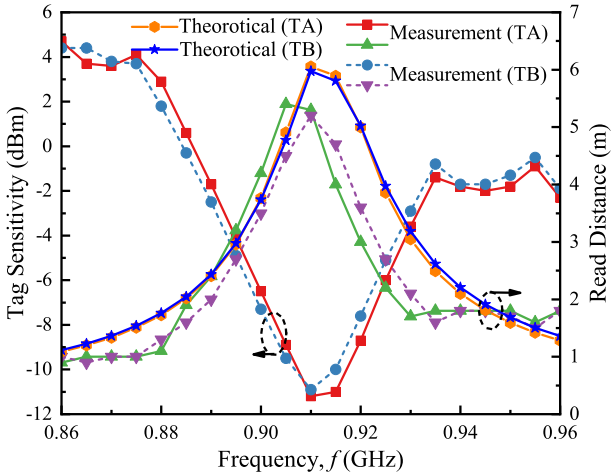

FIGURE 11. Measured tag sensitivities, measured read distances, and theoretical read distances of the proposed tag antenna.

3.28 W. G_r is the realized gain of the tag antenna, τ is the power transfer efficiency of the tag antenna, and P_{ic} is the minimum power required to activate the tag chip. The calculation formula is as follows

$$R = \frac{\lambda}{4\pi}\sqrt{\frac{P_{EIRP}G_r\tau}{P_{ic}}} \tag{1}$$

The calculated read distances for TA and TB states of the tag antenna at 913 MHz are 6.1 m and 6.0 m, respectively. The measured tag sensitivities, measured read distances, and theoretical read distances are shown in Fig. 11. The tag antenna in the TA state shows the lowest sensitivity of -11.2 dBm at 910 MHz, with a maximum read distance of 5.4 m. In the TB state, the lowest sensitivity is -10.9 dBm at 910 MHz, with a maximum read distance of 5.2 m. The maximum measured reading distances in TA and TB states are observed to be 0.7 m and 0.8 m lower than the corresponding theoretical calculated values, respectively. The differences may be attributed to errors in manufacturing, measurement, and the frequency-dependent impedance variation of the tag chip.

Figure 12 shows the simulated and measured read distances of the proposed tag antenna in the xoy and xoz planes. With reference to Fig. 12(a), for measurements in the xoy plane, the tag antenna achieves the maximum reading distance at $\phi = 170°$ and 350°. Both TA and TB states can achieve read distances that exceed 4 m within the angular ranges of $0° < \phi < 30°$, $130° < \phi < 210°$, and $320° < \phi < 360°$. Referring to Fig. 12(b), for measurements in the xoz planes, the maximum reading distance is obtained at $\theta = 0°$. In the angular range of $0° < \theta < 30°$ and $320° < \theta < 360°$, both TA and TB states can achieve a read distance exceeding 4 m. Due to the presence of the backing metal plate, radiation is mainly distributed in the upper half-plane.

Table 1 compares the tag antenna proposed in this paper with recently reported anti-metal tag antennas. The maximum read distance of the tag antenna in this study is comparable to those in references [9] and [20], while the proposed tag antenna has a lower profile. Despite the tag antennas in references [21] and [22] exhibit higher read distances in a metallic environ-

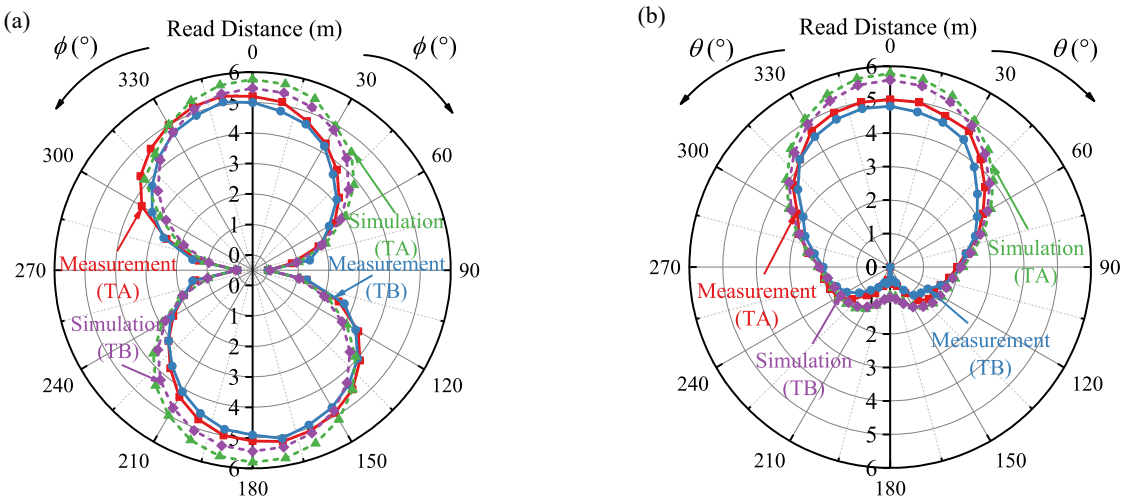

FIGURE 12. Simulated and measured read distances of the proposed tag antenna in the (a) xoy and (b) xoz planes.

TABLE 1. Various parameters comparison of the proposed antenna with few previous reported antenna.

Ref.	Tag Dimension (mm)	Tag Volume (mm^3)	Chip Sensitivity (dBm)	Power (EIRP)	No. of Usable Sides	Max Read Range (m)
This work	$38 \times 20 \times 1.15$	874	-20	3.28 W	2	5.4/5.2
[9]	$42 \times 50 \times 1.6$	3360	-20	4 W	1	5.2
[10]	$40 \times 40 \times 1.6$	2560	-20	3.28 W	1	5.0
[15]	$52 \times 13 \times 2$	1352	-18	4 W	2	7.4/4.9
[16]	$35 \times 22 \times 2.15$	1655.5	-20	4 W	2	6.23/6.08
[20]	$38 \times 38 \times 1.6$	2310.4	-17.8	4 W	1	5.3–5.7
[21]	$40 \times 40 \times 3.1$	4960	-22	4 W	1	6.9
[22]	$30 \times 30 \times 3.0$	2700	-22.9	4 W	1	6.4
[23]	$30 \times 30 \times 1.6$	1440	-19.9	4 W	1	3.5

ment, the proposed tag antenna has a smaller dimension. Compared to the tag antennas in references [10] and [23], the proposed tag antenna achieves a longer read distance. Particularly, the above reference tag antennas can only be used on one side, while the proposed tag antenna can touch metal objects on both sides and maintains consistent anti-metal properties. The tags in references [15] and [16] are also double-sided anti-metal tags, but the proposed tag antenna has a lower profile and better double-sided consistency. Additionally, the proposed tag antenna utilizes soft foam and PET film, providing flexibility to the structure. The antenna structure does not require any shorted vias or parasitic components, making it simple, cost-effective, and easy to design, which is promising for widespread application in the industrial internet of things field.

4. CONCLUSION

This paper proposes a low-profile folded tag antenna with double-sided anti-metal characteristics. The tag antenna uses two shorting stubs to connect three metallic layers, reducing the resonance frequency and achieving a compact size. The middle layer radiation patch loads a rectangular loop structure, effectively expanding the antenna's bandwidth and optimizes impedance matching. The measured maximum read distances are 5.4 m and 5.2 m respectively, indicating excellent anti-metal properties of the tag antenna. It has been demonstrated that the proposed double-sided anti-metal tag antenna can generate stable reading patterns while maintaining consistency in performance between the TA and TB states. Overall, the proposed tag antenna provides a promising solution for anti-metal tag design, demonstrating reliable double-sided anti-metal properties and longer read distances.

ACKNOWLEDGEMENT

This work was supported in part by the Major Science and Technology Project of Fuzhou city, China, under Grant 2022ZD002.

REFERENCES

[1] Hong, J. H., C.-W. Chiu, and H.-C. Wang, "Design of circularly polarized tag antenna with artificial magnetic conductor for on-

body applications," *Progress In Electromagnetics Research C*, Vol. 81, 89–99, 2018.

[2] Yan, Z., S. Lu, C. Zhang, and Z. Yang, "Design and implementation of long-distance dual PIFA antenna structure of small embedded metal UHF RFID tag," *Progress In Electromagnetics Research C*, Vol. 116, 95–112, 2021.

[3] Ma, Y., H. Ning, W. Meng, and C. Tian, "Design and evaluation of a planar I-shaped folded-patch antenna for compact passive UHF RFID tags to cohere on metal," *Progress In Electromagnetics Research Letters*, Vol. 94, 49–55, 2020.

[4] Liu, Q., S. Zhong, Y. Yu, W.-S. Zhao, and G. Wang, "Platform-tolerant nested-slot RFID tag antenna based on jigsaw-shaped metasurface," *IEEE Antennas and Wireless Propagation Letters*, Vol. 21, No. 5, 943–947, May 2022.

[5] Li, X., G. Gao, H. Zhu, Q. Li, N. Zhang, and Z. Qi, "UHF RFID tag antenna based on the DLS-EBG structure for metallic objects," *IET Microwaves, Antennas & Propagation*, Vol. 14, No. 7, 567–572, Mar. 2020.

[6] Faudzi, N. M., M. T. Ali, I. Ismail, H. Jumaat, and N. H. M. Sukaimi, "Compact microstrip patch UHF-RFID tag antenna for metal object," in *2014 IEEE Symposium on Wireless Technology and Applications (ISWTA)*, 160–164, Dec. 2014.

[7] He, Y. and H. Zhang, "A new UHF anti-metal RFID tag antenna design with open-circuited stub feed," in *2013 IEEE International Conference on Communications (ICC)*, 5809–5813, Nov. 2013.

[8] Yang, E. S. and H.-W. Son, "Dual-polarised metal-mountable UHF RFID tag antenna for polarisation diversity," *Electronics Letters*, Vol. 52, No. 7, 496–498, Apr. 2016.

[9] Lee, S.-R., E.-H. Lim, F.-L. Bong, and B.-K. Chung, "Slotted folded patch antenna with double-T-slots for platform-insensitive UHF tag design," *IEEE Transactions on Antennas and Propagation*, Vol. 67, No. 1, 670–675, Jan. 2019.

[10] Ng, W.-H., E.-H. Lim, F.-L. Bong, and B.-K. Chung, "Folded patch antenna with tunable inductive slots and stubs for UHF tag design," *IEEE Transactions on Antennas and Propagation*, Vol. 66, No. 6, 2799–2806, Jun. 2018.

[11] Bong, F.-L., E.-H. Lim, and F.-L. Lo, "Flexible folded-patch antenna with serrated edges for metal-mountable UHF RFID tag," *IEEE Transactions on Antennas and Propagation*, Vol. 65, No. 2, 873–877, 2017.

[12] Zhang, Y. J., D. Wang, and M. S. Tong, "An adjustable quarter-wavelength meandered dipole antenna with slotted ground for metallically and airily mounted RFID tag," *IEEE Transactions on Antennas and Propagation*, Vol. 65, No. 6, 2890–2898, Jun. 2017.

[13] Murugesh, M., E.-H. Lim, P.-S. Chee, and F.-L. Bong, "Complementarily coupled C-shaped microstrip patches with wide-range frequency tuning capability for metal-applicable UHF RFID tag design," *IEEE Transactions on Antennas and Propagation*, Vol. 70, No. 12, 11 548–11 558, 2022.

[14] Lee, S.-R., W.-H. Ng, E.-H. Lim, and S. K. A. Rahim, "Loop-coupled small antenna with enhanced bandwidth for on-metal UHF RFID tag design," *IEEE Transactions on Antennas and Propagation*, Vol. 71, No. 4, 3660–3664, Apr. 2023.

[15] Zheng, J., J. Yuan, and Z. Chen, "A compact UHF RFID tag antenna for anti-metal used on both sides," in *2020 Cross Strait Radio Science & Wireless Technology Conference (CSRSWTC)*, 1–3, Dec. 2020.

[16] Niu, C., J. Yuan, and Z. Xu, "A compact folded RFID tag antenna with nested deformable rings for two-side anti-metal application," *Progress In Electromagnetics Research C*, Vol. 125, 191–200, Oct. 2022.

[17] Erman, F., S. Koziel, and L. Leifsson, "Broadband/Dual-band metal-mountable UHF RFID tag antennas: A systematic review, taxonomy analysis, standards of seamless RFID system operation, supporting iot implementations, recommendations and future directions," *IEEE Internet of Things Journal*, Vol. 10, No. 16, 14 780–14 797, 2023.

[18] Faudzi, N. M., M. T. Ali, I. Ismail, H. Jumaat, and N. H. M. Sukaimi, "Compact microstrip patch UHF-RFID tag antenna for metal object," in *2014 IEEE Symposium on Wireless Technology and Applications (ISWTA)*, 160–164, 2014.

[19] Ltd., V., *Tagformance Pro Measurement System, Manual Tagformance 13.5*, 2023.

[20] Lee, S.-R., W.-H. Ng, E.-H. Lim, F.-L. Bong, and B.-K. Chung, "Compact magnetic loop antenna for omnidirectional on-metal UHF tag design," *IEEE Transactions on Antennas and Propagation*, Vol. 68, No. 2, 765–772, 2020.

[21] Chiang, S.-M., T.-L. Lee, E.-H. Lim, P.-S. Chee, Y.-H. Lee, F.-L. Bong, Y.-N. Phua, and B.-K. Chung, "Miniature folded dipole in rotational symmetry for metal tag design," *Progress In Electromagnetics Research C*, Vol. 110, 55–66, 2021.

[22] Nguyen, M.-T., Y.-F. Lin, C.-H. Chang, C.-H. Chen, and H.-M. Chen, "Compact shorted C-shaped patch antenna for ultra-high frequency radio frequency identification tags mounted on a metallic plate," *International Journal of RF and Microwave Computer-Aided Engineering*, Vol. 31, No. 6, e22595, 2021.

[23] Bong, F.-L., E.-H. Lim, and F.-L. Lo, "Compact orientation insensitive dipolar patch for metal-mountable UHF RFID tag design," *IEEE Transactions on Antennas and Propagation*, Vol. 66, No. 4, 1788–1795, 2018.

[24] Virtanen, J., T. Björninen, L. Ukkonen, and L. Sydänheimo, "Passive UHF inkjet-printed narrow-line RFID tags," *IEEE Antennas and Wireless Propagation Letters*, Vol. 9, 440–443, 2010.